ACS APPLIED MATERIALS & INTERFACES

Letter

www.acsami.org

Bacterial Nanometric Amorphous Fe-Based Oxide: A Potential Lithium-Ion Battery Anode Material

Hideki Hashimoto,[†] Genki Kobayashi,[‡] Ryo Sakuma,[†] Tatsuo Fujii,[†] Naoaki Hayashi,[§] Tomoko Suzuki,[†] Ryoji Kanno,[⊥] Mikio Takano,[§] and Jun Takada*[,†,#]

[†]Graduate School of Natural Science and Technology, Okayama University, Okayama 700-8530, Japan

[‡]Research Center of Integrative Molecular Systems, Institute for Molecular Science, Okazaki, Aichi 444-8585, Japan

[§]Institute for Integrated Cell-Material Sciences, Kyoto University, Sakyo-ku, Kyoto 606-8501, Japan

[⊥]Interdisciplinary Graduate School of Science and Engineering, Tokyo Institute of Technology, Kanagawa 226-850, Japan

[#]CREST, Japan Science and Technology Agency (JST), Okayama 700-8530, Japan

Supporting Information

ABSTRACT: Amorphous Fe^{3+}-based oxide nanoparticles produced by *Leptothrix ochracea*, aquatic bacteria living worldwide, show a potential as an Fe^{3+}/Fe^{0} conversion anode material for lithium-ion batteries. The presence of minor components, Si and P, in the original nanoparticles leads to a specific electrode architecture with Fe-based electrochemical centers embedded in a Si, P-based amorphous matrix.

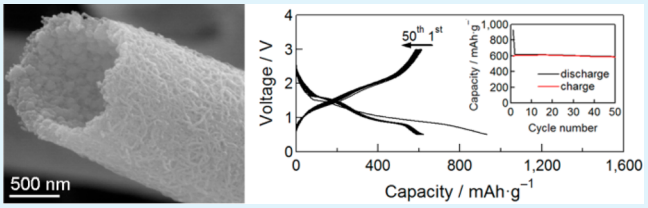

KEYWORDS: *nanoparticles, iron-oxidizing bacteria, bacterial iron oxides, lithium-ion batteries, anode material*

Lithium-ion batteries have become a commonplace power source for portable electronic devices. Application of these batteries is still expanding widely, even to transportation and electric power storage. To meet an increasing variety of application in the future, further exploration of new electrode materials is a very important issue.[1−5] The new material to be proposed in the present work is nanometric amorphous oxide particles produced by *Leptothrix ochracea*, a species of aquatic bacteria living worldwide, in which iron, silicon, and phosphorus are mixed atomically. In the initial discharge process, a specific composite is formed where the Fe-based active species are embedded in an amorphous Si, P-oxide matrix.

Microbes often create mineral deposits that feature elaborate structures and unique compositions.[6−13] For example, two types of aquatic iron-oxidizing bacteria, *Leptothrix ochracea* and *Gallionella ferruginea*, essentially produce the same Fe^{3+}-based amorphous oxide particles (Fe:Si:P ∼73:22:5 in at %, typically; ∼3 nm in diameter) but assemble them in different forms of tubules and twisted fiber bundles, respectively.[10−13] To date, studies of these types of biogenous iron oxides (BIOXs) have mostly been implemented from bacteriological and geochemical perspectives,[6−9] but we have characterized them on the basis of solid-state chemistry and have identified their functionality on the basis of materials science.[10−17] In this study, we have focused on *Leptothrix ochracea*'s product (*L*-BIOX), which can be identified as ocher deposits in natural streams (Figure 1a), irrigation canals, ditches, and even near ocean hydrothermal vents.[6,7] The *L*-BIOX obtained from a water purifying tank in Joyo, Japan[10−12,14−17] have already been shown to have a number of potential applications, including catalyst supports,[12] carriers for cell culture,[14] battery electrodes,[15,16] and precursors for pigments.[17]

The tubules have a fixed bore diameter of ∼1 μm and a variable length of up to several centimeters, as observed by scanning electron microscopy (SEM, Figure 1b, c). Such a structure results because the nanometric oxide particles precipitate on an extracellular microtubular template made of bacterial organic excrement (Figure 1d).[18,19] The outer surface of each tubule is covered with ∼20 nm wide and 50−100 nm long fibrils, whereas the inner surface is composed of 20−120 nm-sized globules (Figure 1e, f, respectively).[18] Although seemingly different from each other, these structural motifs share common primary particles (∼3 nm in diameter),[12] such as those indicated by the red arrowheads in the insets in Figure 1e, f (images taken using C_s-corrected scanning transmission electron microscopy (STEM)). The roughness of these motifs due to jutting or missing primary particles suggests loose connections of the primary particles. Therefore, the *L*-BIOX tubules are hierarchical (nano−meso−micro) with respect to both their framework and clearance, and the surface area of the tubules is 280 m^2/g.[12]

The chemical composition of *L*-BIOX determined via energy-dispersive X-ray spectroscopy (EDX), thermogravimetry (TG), and inductively coupled plasma-optical emission spectrometry (ICP-OES) can be approximately expressed as

Received: February 12, 2014
Accepted: April 1, 2014
Published: April 1, 2014

   dx.doi.org/10.1021/am500905y | *ACS Appl. Mater. Interfaces* 2014, 6, 5374−5378

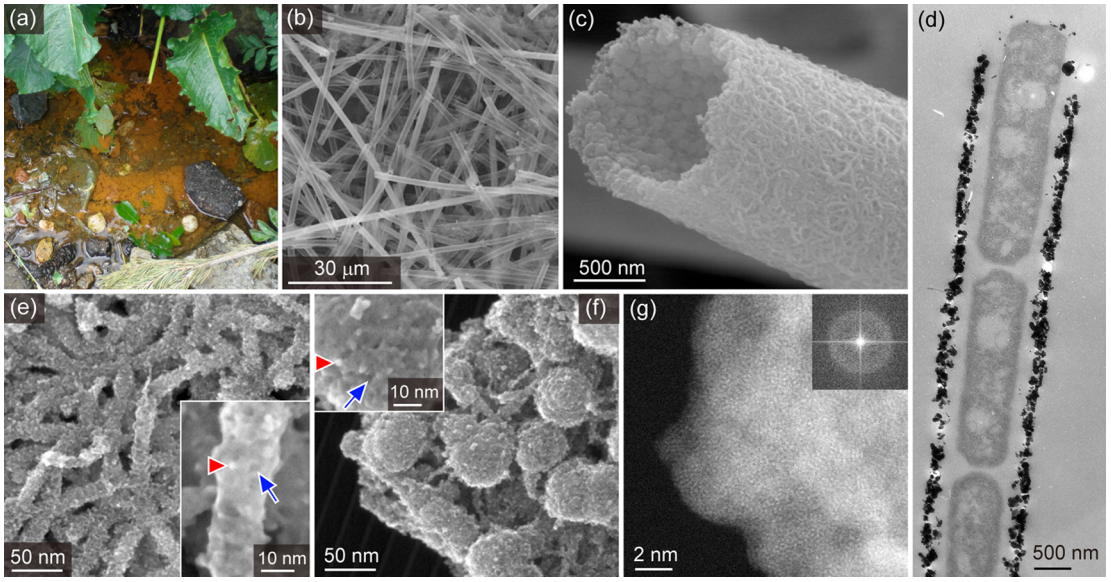

Figure 1. Photograph and micrographs of *L*-BIOX. (a) Ocher *L*-BIOX produced in a stream. (b) Low- and (c) high-magnification SEM images of *L*-BIOX. (d) TEM image showing the early stage formation of *L*-BIOX around rod-like bacterial cells lined up head to tail (for details see the TEM observations of the Bacteria subsection in the Methods section of the Supporting Information). (e, f) C_s-corrected STEM images of the fibrillar and globular motifs of the outer and inner surfaces, respectively. Every tubule is made up of common primary particles (~3 nm in diameter), similar to those indicated with the red arrowheads in the insets of e and f. Sites where the primary particles are missing are indicated with blue arrows. (g) High-resolution HAADF-STEM image of the primary particles showing a uniform, segregation-free elemental distribution. Inset: 2D Fourier transform image with a theoretical electron probe size of 0.1 nm.

$15Fe_2O_3{\cdot}8SiO_2{\cdot}P_2O_5{\cdot}30H_2O$ (Fe:Si:P ~73:22:5 in at %).[11] EDX measurements of sectioned tubular walls of *L*-BIOX indicate compositional homogeneity over the structure, internally and externally, at a nanometer resolution (see the Supporting Information, Figure S1a–f). Higher-resolution examinations with high-angle annular dark field-STEM (HAADF-STEM) using an electron probe converged to 0.1 nm yielded consistent results without any sign of elemental segregation (Figure 1g). The amorphous nature of the primary particles should also be noted. The 2D Fourier transformation images (inset to Figure 1g) are spot-free halo patterns, revealing an amorphous structure at a resolution of up to ~1 nm (see also the Supporting Information, Figure S1 g, h and Figure S2). Therefore, it is clear that the 3 nm wide particles containing ~560 Fe, ~170 Si, and ~40 P atoms, are the compositional and structural unit throughout the *L*-BIOX tubules. Here we show that these nanometric primary particles show electrochemical properties suitable for lithium-ion batterries.

Nanosizing and appropriate surface modification of electrode materials are the most recent approaches for improving their energy density, cyclability, and power rate,[4,5] but these techniques generally require complicated and costly processes that present stumbling blocks for their practical application. Therefore, it would be quite significant if the primary *L*-BIOX particles, which are produced in the form of easily handled tubules simply by exposing Fe-containing groundwater to air, are high performing. The expected capacity for the Fe^{3+}/Fe^0 conversion process is 666 mAh/g based on the composition of *L*-BIOX (Fe 8.3 mmol/g). Figure 2 presents experimental discharge–charge curves for simple *L*-BIOX/Li-metal cells taken at two largely different current rates of 33.3 mA/g (0.05 C) and 666 mA/g (1 C) in the voltage range 0–3 V over 10–50 cycles. For these experiments, the working electrode consisted of a simple, ball-milled mixture of dried *L*-BIOX

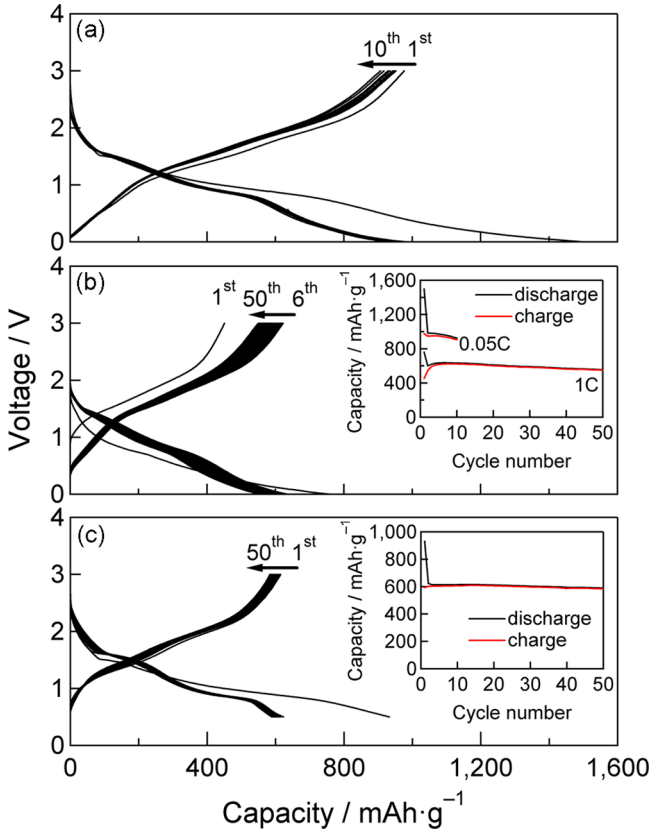

Figure 2. Discharge–charge performance of different current rates and potential ranges. (a) Discharge–charge curves at 33.3 mA/g (0.05 C) between 0 and 3.0 V. (b) Discharge–charge curves at 666 mA/g (1 C) between 0 and 3.0 V. (c) Discharge–charge curves at 33.3 mA/g (0.05 C) between 0.5 and 3.0 V. Insets show the cycle-life performance.

dx.doi.org/10.1021/am500905y | ACS Appl. Mater. Interfaces 2014, 6, 5374–5378

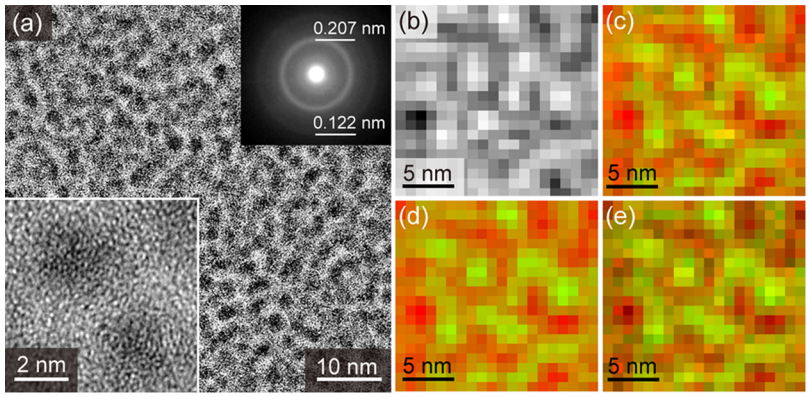

Figure 3. TEM images for the first discharge process at 0.05 C down to 0 V. (a) Low-magnification TEM image of the *L*-BIOX electrode. Upper inset: electron diffraction pattern taken from an area containing ~100 fine particles. Lower inset: high-resolution image of one pair of the black dots seen in a. (b) High-magnification HAADF-STEM image. (c) Distribution map of Fe (green) and Li (red). (d) Distribution map of Fe (green) and O (red). (e) Distribution map of Fe (green) and Si (red).

tubules, a conventional carbon material, and a binder (For details see the Electrochemical Measurements section in the Supporting Information, S1). Here a discharge (charge) process corresponds to the transport of Li^+ ions from (to) the Li foil to (from) *L*-BIOX, and a rate of *n*C corresponds to a full discharge or charge in $1/n$ h. As can be seen in Figure 2a, the first discharge down to 0 V at 0.05 C extended to an unreasonably high capacity of ~1500 mAh/g, which was most probably an extrinsic phenomenon resulting from the formation of the solid–electrolyte interface.[20,21] For the second and subsequent cycles, a reduced yet rather high reversible capacity of ~900 mAh/g was observed. Moreover, at the 20-fold current rate of 1 C, a capacity of ~550 mAh/g was maintained over 50 cycles (Figure 2b). Even when the voltage range was limited to 0.5–3.0 V (0.05 C, Figure 2c), where the likely anxiety of Li-metal deposition at lower voltages was eliminated, a capacity of ~600 mAh/g was maintained over at least 50 cycles.

In control experiments using an *L*-BIOX-free electrode, it was found that carbon makes a remarkable contribution of 200 mAh/g to the total capacity of 900 mAh/g at 0.05 C. A pseudocapacity effect involving the electrolyte is another possible factor increasing the total capacity. Conversion reactions typically involve electrolyte decomposition in the low-voltage region to form polymeric/gel films exhibiting a pseudocapacity effect, which amounts to ~150 mAh/g in the case of CoO.[22,23] In the present system, the decrease in capacity down to ~600 mAh/g for the voltage range limited to 0.5–3 V thus seems to be caused by the effects of the carbon and the electrolyte.

To track the electrochemical process, the most convenient XRD method proved to be of no use because not only the starting materials but also presumably the resulting products were nanometric and amorphous. However, the behavior of the most important active species, Fe, could be analyzed by TEM and ^{57}Fe Mössbauer spectroscopy.[24,25] As can be seen in the typical TEM image shown in Figure 3a of a sample after the first discharge process down to 0 V at 0.05 C, extremely small particles with diameters of ~2 nm were densely dispersed in a matrix. These particles exhibited very broad double diffraction rings (upper inset to Figure 3a), but no clear lattice fringes in the high resolution TEM image (lower inset to Figure 3a). The lattice spacings estimated from the ring pattern, 0.122 and 0.207 nm, were close to d_{112} = 0.1170 nm and d_{110} = 0.2027 nm for metallic iron, α-Fe (PDF 00–006–0696 (ICDD, 2009)). This result indicated the formation of fairly pure but poorly crystalline α-Fe nanoparticles, which is consistent with the Mössbauer results (see the Supporting Information, S3). The signals for "Fe," "Li," "O," and "Si" for elemental mapping by electron energy loss spectroscopy were sufficiently strong to reveal a pronounced tendency of the separation of "Fe" from "Li," "O," and "Si" (Figure 3c–e). The signal for "P" fell below the measurable limits. Therefore, the first discharge process essentially involves the conversion of the loose aggregate of *L*-BIOX nanoparticles (~560 Fe, ~170 Si, and ~40 P atoms/particle) into a composite of poorly crystalline α-Fe-like nanoparticles (~360 Fe atoms/particle) embedded in a Li-, Si-, and probably P-containing amorphous oxide matrix.

If the Si^{4+} and P^{5+} ions mixed in the original *L*-BIOX primary particles were converted to Si^0 and P^0, respectively, their presence would help increase the capacity; however, preliminary soft X-ray absorption near edge structure measurements suggested that their contribution was very minor, if any. Rather, it is believed that Si and P contribute to the high cyclability and high rate capability after the first discharge by inhibiting the contact and growth of the nanosized Fe species and providing Li ions with a three-dimensional network of pathways for closely approaching the Fe-based centers during discharging and easily leaving during charging. Of course, the Fe oxide that reforms during the first charge process must differ in both composition (essentially free from Si and P) and structure from the original *L*-BIOX primary particles. The repeated change of the nanometric Fe-containing species between contracted α-Fe-like particles and swollen Fe^{3+}-oxide particles must be more or less compensated by a reverse volume change in the amorphous, and therefore flexible, Si, P-oxide matrix that stores and releases Li^+ and O^{2-} ions.

The best-studied Fe^{3+}/Fe^0 conversion material is α-Fe_2O_3.[25−32] This oxide has a high theoretical capacity (~1000 mAh/g) and also high chemical stability, abundance, and low toxicity, which together enable easy control of its particle morphology and high productivity.[25−32] The study by Chen et al. is instructive.[29] They addressed the most important issue of poor cyclability caused by the very large volume change of ~96% during the α-Fe_2O_3–α-$LiFe_2O_3$–$Li_2Fe_2O_3$–Fe discharge/charge processes[30] and concluded that the use of single-crystalline nanotubes was the best solution because of their shape-preserving capability. Moit et al.[31] worked on a

hollow and porous shell made of α-Fe_2O_3 nanoparticles, resulting from thermal decomposition of a precursory composite obtained by using a species of bacteria for shape forming, and concluded that the high porosity and stable particle connectivity drastically improved the performance of α-Fe_2O_3. *L*-BIOX is a new material and there is still scope for further improvement. The original *L*-BIOX tubules are destroyed in the process of mixing with the carbon and binder. Preservation of the original tubular shape is another possibility to be pursed for improvement.

Optimization of electrode architecture is an important target of electrode materials research. Intimate hybridization with carbon materials like conductive carbon nanofibers[32] has been the most common measure to improve the performance of Fe_2O_3. In the present architecture the nanometric Fe-based electrochemical centers seem to be intimately linked to the amorphous and therefore flexible Li-transporting network. A similar composite structure was reported by Idota et al. for a Sn-based electrode material.[33] They succeeded in drastically improving the cyclability by dispersing the tin oxide particles in a glassy B^{3+}-, P^{5+}-, and Al^{3+}-oxide matrix. It is interesting that *L*-BIOX naturally provides this kind of advantageous composite architecture. As a matter of course the discharge−charge curves of *L*-BIOX are considerably different from those of α-Fe_2O_3. The latter oxide normally shows a single extended plateau at ∼1 V,[25−32] whereas *L*-BIOX does double small plateaus at ∼1.5 and ∼1 V. The details are under investigation using various analytical methods.

Another noteworthy feature of *L*-BIOX is that it can be ceaselessly produced at a high rate and at an extremely low cost. Even in our small plant (see the Supporting Information, Figure S4), ∼160 g of *L*-BIOX and ∼6200 L of Fe-free water can be obtained in 1 day simply by exposing that amount of natural groundwater to the outside environment. *L*-BIOX is, obviously, an extremely cost-effective, beneficial material. The relationship between the chemical composition of the water supplied to *Leptothrix ochracea* and the composition of the product is currently under investigation. The development of a synthetic process for fine control of the particle morphology, chemical composition, particle aggregation, and other factors is also under exploration.

In summary, we have proposed a unique approach for the development of new battery materials, which we noticed in the course of our basic and general study of iron oxide materials produced by bacteria. Relatively high capacity and good cyclability were found for *L*-BIOX, which was used as produced, by simple washing and drying steps. The positive result for *L*-BIOX as an anode material for Li-ion batteries is yet an example indicating that BIOXs are an unexplored frontier in solid-state chemistry and materials science. However, we believe that the development of a related artificial synthetic process that enables fine control is also worth exploring.

■ ASSOCIATED CONTENT

Supporting Information

Experimental details, characterization of the sample, ex situ Mossbauer results, and sample collection procedures are available free of charge via the Internet at http://pubs.acs.org.

■ AUTHOR INFORMATION

Corresponding Author

*E-mail: jtakada@cc.okayama-u.ac.jp.

Notes

The authors declare no competing financial interest.

■ ACKNOWLEDGMENTS

We thank H. Asaoka, Y. Watanabe, H. Ishihara, Y. Kusano, Y. Ikeda, M. Nakanishi, H. Kunoh, M. Seno, K. Ida, T. Nishimori, R. Miyake, and M. Furutani for their helpful discussions. This study was financially supported by the Special Funds for Education and Research from the Ministry of Education, Culture, Sports, Science, and Technology and JSPS KAKENHI Grant Number 22860040, 24760550, and 23360309.

■ REFERENCES

(1) Tarascon, J. M.; Armand, M. Issues and Challenges Facing Rechargeable Lithium Batteries. *Nature* **2001**, *414*, 359−367.
(2) Goodenough, J. B.; Kim, Y. Challenges for Rechargeable Li Batteries. *Chem. Mater.* **2010**, *22* (3), 587−603.
(3) Ellis, B. L.; Lee, K. T.; Nazar, L. F. Positive Electrode Materials for Li-Ion and Li-Batteries. *Chem. Mater.* **2010**, *22* (3), 691−714.
(4) Bruce, P. G.; Scrosati, B.; Tarascon, J. M. Nanomaterials for Rechargeable Lithium Batteries. *Angew. Chem., Int. Ed.* **2008**, *47* (16), 2930−2946.
(5) Arico, A. S.; Bruce, P.; Scrosati, B.; Tarascon, J. M.; Schalkwijk, W. V. Nanostructured Materials for Advanced Energy Conversion and Storage Devices. *Nat. Mater.* **2005**, *4*, 366−377.
(6) Emerson, D.; Fleming, E. J.; McBeth, J. M. Iron-Oxidizing Bacteria: An Environmental and Genomic Perspective. *Annu. Rev. Microbiol.* **2010**, *64*, 561−583.
(7) Spring, S., The Genera *Leptothrix* and *Sphaerotilus*. In *The Prokaryotes*; Dworkin, M., Falkow, S., Rosenberg, E., Schleifer, K. H., Stackebrandt, E., Eds.; Springer: New York, 2006; Vol. *5*, pp 758−777.
(8) Chan, C. S.; De Stasio, G.; Welch, S. A.; Girasole, M.; Frazer, B. H.; Nesterova, M. V.; Fakra, S.; Banfield, J. F. Microbial Polysaccharides Template Assembly of Nanocrystal Fibers. *Science* **2004**, *303* (5664), 1656−1658.
(9) Ferris, F. G. Biogeochemical Properties of Bacteriogenic Iron Oxides. *Geomicrobiol. J.* **2005**, *22* (3−4), 79−85.
(10) Hashimoto, H.; Yokoyama, S.; Asaoka, H.; Kusano, Y.; Ikeda, Y.; Seno, M.; Takada, J.; Fujii, T.; Nakanishi, M.; Murakami, R. Characteristics of Hollow Microtubes Consisting of Amorphous Iron Oxide Nanoparticles Produced by Iron Oxidizing Bacteria *Leptothrix ochracea*. *J. Magn. Magn. Mater.* **2007**, *310* (2), 2405−2407.
(11) Hashimoto, H.; Fujii, T.; Kohara, S.; Asaoka, H.; Kusano, Y.; Ikeda, Y.; Nakanishi, M.; Benino, Y.; Nanba, T.; Takada, J. Amorphous Structure of Iron Oxide of Bacterial Origin. *Mater. Chem. Phys.* **2012**, *137* (2), 571−575.
(12) Ema, T.; Miyazaki, Y.; Kozuki, I.; Sakai, T.; Hashimoto, H.; Takada, J. Highly Active Lipase Immobilized on Biogenous Iron Oxide via an Organic Bridging Group: The Dramatic Effect of the Immobilization Support on Enzymatic Function. *Green Chem.* **2011**, *13* (11), 3187−3195.
(13) Suzuki, T.; Hashimoto, H.; Itadani, A.; Matsumoto, N.; Kunoh, H.; Takada, J. Silicon and Phosphorus Linkage with Iron via Oxygen in the Amorphous Matrix of *Gallionella ferruginea* stalks. *Appl. Environ. Microbiol.* **2012**, *78* (1), 236−241.
(14) Seno, M.; Kasai, T.; Takada, J.; Hashimoto, H.; Suzuki, T. Japan patent Tokugan JP 2012−181690 (2012). The potential as a carrier for cell culture was publicized in the form of patent.
(15) Takada, J.; Fujii, T.; Nakanishi, M. Japan patent Tokkai JP 2008−177061 (2008). The potential as a cathode material was publicized in the form of patent.
(16) Takada, J.; Hashimoto, H.; Fujii, T.; Nakanishi, M.; Kanno, R.; Kobayashi, G.; Takano, M. PCT/JP 2012−83866 (2012). The potential as an anode material was publicized in the form of patent.
(17) Hashimoto, H.; Asaoka, H.; Nakano, T.; Kusano, Y.; Ishihara, H.; Ikeda, Y.; Nakanishi, M.; Fujii, T.; Yokoyama, T.; Horiishi, N.; Nanba, T.; Takada, J. Preparation, Microstructure, and Colour Tone of Microtubule Material Composed of Hematite/Amorphous-Silicate

Nanocomposite from Iron Oxide of Bacterial Origin. *Dyes Pigm.* **2012**, *95* (3), 639−643.
(18) Suzuki, T.; Hashimoto, H.; Ishihara, H.; Kasai, T.; Kunoh, H.; Takada, J. Structural and Spatial Associations Between Fe, O, and C in the Network Structure of the *Leptothrix ochracea* Sheath Surface. *Appl. Environ. Microbiol.* **2011**, *77* (21), 7873−7875.
(19) Furutani, M. Assemblage of Bacterial Saccharic Microfibrils in Sheath Skeleton Formed by Cultured *Leptothrix* sp. Strain OUMS1. *J. Mar. Sci.: Res. Dev.* **2011**, *S:5*, 5.
(20) Balaya, P.; Li, H.; Kienle, L.; Maier, J. Fully Reversible Homogeneous and Heterogeneous Li storage in RuO_2 with High Capacity. *Adv. Funct. Mater.* **2003**, *13* (8), 621−625.
(21) Maier, J. Nanoionics: Ion Transport and Electrochemical Storage in Confined Systems. *Nat. Mater.* **2005**, *4*, 805−815.
(22) Poizot, P.; Laruelle, S.; Grugeon, S.; Dupont, L.; Tarascon, J. M. Nano Sized Transition Metal Oxides as Negative Electrode Materials for Lithium Ion Batteries. *Nature* **2000**, *407*, 496−499.
(23) Laruelle, S.; Grugeon, S.; Poizot, P.; Dollé, M.; Dupont, L.; Tarascon, J. M. On the Origin of the Extra Electrochemical Capacity Displayed by MO/Li Cells at Low Potential. *J. Electrochem. Soc.* **2002**, *149* (5), A627−A634.
(24) Greenwood, N. N.; Gibb, T. D. *Mössbauer Spectroscopy*; Chapman and Hall: London, 1971; p 659.
(25) Larcher, D.; Bonnin, D.; Cortes, R.; Rivals, I.; Personnaz, L.; Tarascon, J. M. Combined XRD, EXAFS, and Mössbauer Studies of the Reduction by Lithium of α-Fe_2O_3 with Various Particle Sizes. *J. Electrochem. Soc.* **2003**, *150* (12), A1643−A1650.
(26) Thackeray, M. M.; David, W. I. F.; Goodenough, J. B. Structural Characterization of the Lithiated Iron Oxides $Li_xFe_3O_4$ and $Li_xFe_2O_3$ ($0 < x < 2$). *Mater. Res. Bull.* **1982**, *17*, 785−793.
(27) Thackeray, M. M.; David, W. I. F.; Goodenough, J. B. High-Temperature Lithiation of α-Fe_2O_3: A Mechanistic Study. *J. Solid State Chem.* **1984**, *55*, 280−286.
(28) Ji, L.; Lin, Z.; Alcoutlabi, M.; Zhang, X. Recent Developments in Nanostructured Anode Materials for Rechargeable Lithium-Ion Batteries. *Energy Environ. Sci.* **2011**, *4* (8), 2682−2699.
(29) Chen, L.; Xu, H.; Li, L. e.; Wu, F.; Yang, J.; Qian, Y. A Comparative Study of Lithium-Storage Performances of Hematite: Nanotubes vs. Nanorods. *J. Power Sources* **2014**, *245*, 429−435.
(30) Ponrouch, A.; Taberna, P.-L.; Simon, P.; Palacín, M. R. On the Origin of the Extra Capacity at Low Potential in Materials for Li Batteries Reacting through Conversion Reaction. *Electrochim. Acta* **2012**, *61*, 13−18.
(31) Miot, J.; Recham, N.; Larcher, D.; Guyot, F.; Brest, J.; Tarascon, J. M. Biomineralized α-Fe_2O_3: Texture and Electrochemical Reaction with Li. *Energy Environ. Sci.* **2014**, *7* (1), 451−460.
(32) Wu, M.-S.; Ou, Y.-H.; Lin, Y.-P. Electrodeposition of Iron Oxide Nanorods on Carbon Nanofiber Scaffolds as an Anode Material for Lithium-Ion Batteries. *Electrochim. Acta* **2010**, *55* (9), 3240−3244.
(33) Idota, Y. Tin-Based Amorphous Oxide: A High-Capacity Lithium-Ion-Storage Material. *Science* **1997**, *276* (5317), 1395−1397.